



BCS-BEC crossover in a two-band superconductor with odd-parity hybridizationG. N. Bremm, M. A. Continentino , and T. Micklitz *Centro Brasileiro de Pesquisas Físicas, Rua Xavier Sigaud 150, 22290-180, Rio de Janeiro, Brazil*

(Received 28 September 2020; revised 16 July 2021; accepted 24 August 2021; published 16 September 2021)

We study the crossover from the weak coupling Bardeen-Cooper-Schrieffer (BCS) state to Bose-Einstein condensation (BEC) at strong coupling in a two-band superconductor with orbitals of opposite parity coexisting at a common Fermi surface in the metallic state. In such systems hybridization can play a role similar to spin-orbit interaction in fermionic spinor gases, enhancing interband pairing and opening the possibility for driving the BCS-BEC crossover. Building on a mean-field analysis, we investigate the BCS-BEC crossover induced by a variation of the hybridization strength. We show that the relevant scale for the crossover depends strongly on the ratio of effective masses, with the crossover favored in systems with one dispersive and one flat band. Including the effect of thermal pair fluctuations in a one-loop approximation, we calculate the dependence of the critical temperature on the microscopic parameters in the strong coupling regime.

DOI: [10.1103/PhysRevB.104.094514](https://doi.org/10.1103/PhysRevB.104.094514)**I. INTRODUCTION**

Multiorbital superconductors have been in the focus of active research for many decades. Starting with the seminal works by Suhl [1] and Kondo [2] on transition metals, the discovery of iron-based high- T_c superconductors has lead to a more recent boost in the interest of superconductors involving multiple orbitals [3–9]. In the early works, a two-gap scenario for a model of decoupled s and d bands has been proposed which has only recently been experimentally observed [10–16]. Hybridization of orbitals, on the other hand, suppresses the possibility of independent intraband pairs and, at the same time, facilitates the formation of interband superconductivity with pairs formed by electrons belonging to different bands [17]. Recent numerical work on a two-orbital model [18,19] for the pnictides, e.g., conclude on the favoring of interorbital pairing, a scenario further investigated in Refs. [20,21]. Interband pairing has also been studied in the context of heavy fermions [22,23], cuprates [24], cold atom systems, and even quantum chromodynamics [25,26].

In the case of heavy fermions, it was argued that interband pairing could occur for f and d electrons. That is, involving bands with largely different effective masses and orbitals of opposite parity [22,23]. The hybridization in this case is odd under parity transformation and shares characteristics of spin orbit interaction, as pointed out in the recent work Ref. [27]. The latter can play an interesting role in driving a BCS-BEC crossover, as recently discussed in the context of ultracold fermionic spinor gases with tunable synthetic SU(2) gauge fields. More specifically, it has been proposed that varying spin orbit interaction allows us to continuously interpolate, at a fixed (weak) interaction strength, between the two scenarios for the formation of the superfluid state in fermionic systems. That is, the Bardeen-Cooper-Schrieffer state (BCS) [28], where weakly coupled Cooper pairs are formed from fermion states near the Fermi level and the characteristic size for the pair correlation significantly exceeds

the interparticle distance, and the Bose-Einstein condensation regime (BEC) [29] where fermions are first paired into compact two-particle ‘molecules,’ which then condense.

Motivated by the (formal) similarities between odd parity hybridization and spin orbit interaction, we here study the possibility of a hybridization driven (e.g., via pressure or doping) BCS-BEC crossover in multiband superconductors [30,31] involving atomic orbitals of opposite parity. An important difference to fermionic spinor gases is the absence of a symmetry constraint relating the involved bands. Specifically, we find that the ratio of effective fermion masses constitutes an important parameter in the present problem [32–35]. Starting out from a model, previously introduced by Khomskii and co-workers to investigate thermodynamic and electrodynamic properties of heavy fermion systems [22,23], we focus on the scattering length, hybridization strength, and ratio of effective masses as relevant parameters for the BCS-BEC crossover. We first study the mean field properties and then include the effect of thermal pair fluctuations in a one-loop approximation to estimate the critical temperature in the strong coupling regime. We find that the hybridization can play a similar role to the scattering length, driving the crossover from the BCS to the BEC regime, where the relevant scale for the crossover depends on the ratio of effective masses. Large ratios favor the crossover, which is specifically interesting for heavy fermion systems with wide d and shallow f bands.

The paper is organized as follows. In Sec. II we introduce the model for the two-band superconductor which is then exposed to a mean-field analysis in Sec. III. We discuss, respectively, the mean-field order parameter, critical temperature, and chemical potential, and compare their dependence on the fermionic scattering length, odd-parity hybridization, and ratio of effective masses. Section IV explores the strong coupling regime. We derive the effective gaussian theory for the two-particle ‘molecules’ from which we calculate the critical temperature in the BEC limit. Throughout the paper we set $k_B = \hbar = 1$.

II. MODEL

We start out from the two-band model $\hat{H} = \hat{H}_0 + \hat{H}_{\text{int}}$, previously introduced by Khomskii and co-workers to study superconductivity in heavy-fermion systems [22,23]. The free fermion Hamiltonian,

$$\hat{H}_0 = \sum_{\mathbf{k}, \sigma} (\epsilon_{\mathbf{k}}^f \hat{f}_{\mathbf{k}\sigma}^\dagger \hat{f}_{\mathbf{k}\sigma} + \epsilon_{\mathbf{k}}^d \hat{d}_{\mathbf{k}\sigma}^\dagger \hat{d}_{\mathbf{k}\sigma} + V_{\mathbf{k}} \hat{f}_{\mathbf{k}\sigma}^\dagger \hat{d}_{\mathbf{k}\sigma} + \text{H.c.}), \quad (1)$$

describes f and d electrons with dispersions $\epsilon_{\mathbf{k}}^f = \mathbf{k}^2/(2m_f)$ and $\epsilon_{\mathbf{k}}^d = \mathbf{k}^2/(2m_d)$, respectively, and hybridizing via the potential $V_{\mathbf{k}}$. Here \hat{f}^\dagger, \hat{f} and \hat{d}^\dagger, \hat{d} are the creation and annihilation operators for f and d electrons, summation is over three-dimensional momenta \mathbf{k} and spin $\sigma = \uparrow, \downarrow$, and ‘H.c.’ denotes the hermitian conjugate. The attractive interaction,

$$\hat{H}_{\text{int}} = \frac{1}{N} \sum_{\mathbf{k}\mathbf{k}', \sigma} g_{\mathbf{k}\mathbf{k}'} \hat{f}_{\mathbf{k}\sigma}^\dagger \hat{d}_{-\mathbf{k}-\sigma}^\dagger \hat{d}_{-\mathbf{k}'-\sigma} \hat{f}_{\mathbf{k}'\sigma}, \quad (2)$$

with local potential $g_{\mathbf{k}\mathbf{k}'} = -g/2$, where g is the (positive) coupling constant and N the number of lattice sites, induces s -wave pairing with (mean-field) order parameter

$$\Delta_0 = \frac{g}{4} \sum_{\mathbf{k}, \sigma} \langle \hat{d}_{-\mathbf{k}-\sigma} \hat{f}_{\mathbf{k}\sigma} \rangle. \quad (3)$$

Notice that in the absence of a hybridization, $\hat{V}_{\mathbf{k}} = 0$, the model only accounts for interband pairing. For finite hybridizations, on the other hand, it includes both inter- and intraband pairing, as evident in the band representation discussed below.

A similar model has recently been discussed for the pnictides [20,21]. However, there the two orbitals involved share the same parity, while for our discussion the opposite parity of d and f orbitals is a crucial ingredient. (A corresponding model with even parity hybridization does not show a BCS-BEC crossover induced by the hybridization, see Ref. [36].) Opposite parity of orbitals implies that the hybridization potential is odd under parity transformation, $V_{-\mathbf{k}} = -V_{\mathbf{k}}$, and the small momentum expansion of the hybridization potential reads $V_{\mathbf{k}} \simeq i\alpha v_F (k_x + k_y + \gamma k_z)$, with v_F the Fermi velocity. Notice that in the strong-coupling limit there are no Fermi surfaces and the Fermi velocity then is a measure for the number density, $v_F \propto n^{1/3}$.

For concreteness we here specified to systems with tetragonal symmetry in which the main interaction between orbitals resides within the layers, as frequently encountered in heavy fermions materials exhibiting nearly two-dimensional behavior [38]. The dimensionless parameter α controls the hybridization strength, and we will focus on cases in which the main overlap between orbitals resides within the layers, i.e., on anisotropies $\gamma \ll 1$. Finally, notice that in a time-reversal invariant system α is a real parameter, and the hybridization potential $V_{\mathbf{k}}$ purely imaginary.

As already discussed in the introduction, the above model Eqs. (1) and (2) share some similarities with fermionic spinor gases with pair correlations and spin orbit interactions. Due to the recent progress in the generation of synthetic SU(2) gauge fields, the latter have been studied in detail [39–44], and the scenario of a BCS-BEC crossover driven by the tunable spin orbit interaction has been suggested [42,45]. Given the

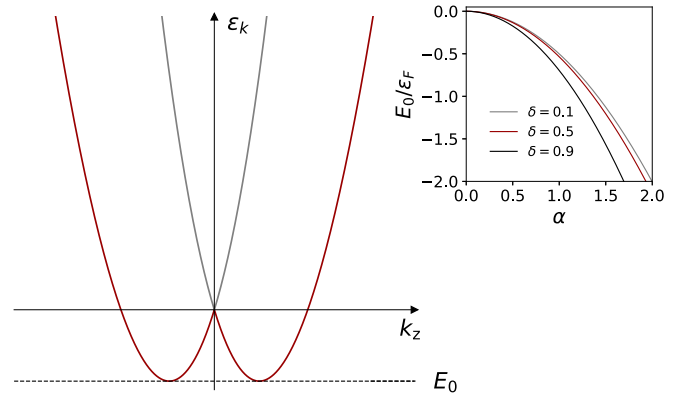


FIG. 1. Schematic plot of the dispersion relation $\epsilon(k_x = k_y = 0, k_z)$ of the two band system in the absence of pairing correlations $\Delta_0 = 0$. Dashed line indicates the energy of the band minimum, $E_0(\delta, \alpha)$, defined in the main text. Inset: $E_0(\delta, \alpha)$ as function of α for different values of δ .

similarities between both systems, it is then natural to investigate a BCS-BEC crossover in the two-band superconductors driven by odd-parity hybridization. An important difference to fermionic spinor gases is the absence of a symmetry constraint on the dispersion relation of bands coupled by the hybridization. While spin orbit interaction couples fermions with identical dispersion (as imposed by time-reversal symmetry), the ratio of fermion masses constitutes a relevant parameter in the present problem. More specifically, we assume that $m_f \geq m_d$ and introduce the ‘difference in fermion masses,’ $\delta = (m_f - m_d)/(m_f + m_d)$, taking values $0 \leq \delta < 1$, and then study pairing as a function of the scattering length (see below), hybridization α , and mass difference δ . We will see that interband pairing in the weak coupling regime is reduced upon increasing δ , while the situation is different in the strong coupling regime. Also, the BCS-BEC crossover driven by moderate hybridization requires rather large mass differences.

For the following it is convenient to introduce the (inverse) reduced mass $2/m \equiv 1/m_f + 1/m_d$, where $\epsilon_F = k_F^2/(2m)$ the Fermi energy and $k_F = k_F^f \sqrt{1 + \delta} = k_F^d \sqrt{1 - \delta}$. Figure 1 shows the single particle dispersion for the two band system Eq. (1) for momenta in the plane $k_z = 0$. The band minimum is at $E_0(\delta, \alpha) = (\alpha/\delta)^2(\sqrt{1 - \delta^2} - 1)\epsilon_F < 0$, which is reduced by increasing either hybridization α or mass difference δ (see inset of Fig. 1). In the presence of pair correlations induced by the attractive interaction Eq. (2), the crossover from the BCS into the BEC regime is expected to occur when the chemical potential falls below this energy $\mu \lesssim E_0$ [46–51].

Following the standard procedure, we introduce a path integral representation for the partition function in terms of a fermionic field integral. Decoupling interactions via Hubbard-Stratonovich transformation and integrating out fermionic degrees of freedom (see Appendix A for details) we arrive at the effective action,

$$S[\Delta] = \frac{2}{g} \sum_q |\Delta_q|^2 - \text{Tr} \ln \mathbf{G}_\Delta^{-1} + C, \quad (4)$$

where $C = \sum_{\mathbf{k}} (\xi_{\mathbf{k}}^d + \xi_{\mathbf{k}}^f)/T$ is a constant, Δ is the pairing field, $q = (\omega_m, \mathbf{q})$ a four-momentum with $\omega_m = 2m\pi T$ (m integer) the bosonic Matsubara frequencies, and the trace accounts for summation over Nambu space and internal degrees of freedom. We further introduced the inverse Nambu-Gorkov Green's function $\mathbf{G}^{-1} = \mathbf{G}_0^{-1} + \Delta$, with

$$\mathbf{G}_{0,k}^{-1} = \begin{pmatrix} i\epsilon_n - \xi_{\mathbf{k}}^f & -\bar{V}_{\mathbf{k}} & 0 & 0 \\ -V_{\mathbf{k}} & i\epsilon_n - \xi_{\mathbf{k}}^d & 0 & 0 \\ 0 & 0 & i\epsilon_n + \xi_{\mathbf{k}}^f & -V_{\mathbf{k}} \\ 0 & 0 & -\bar{V}_{\mathbf{k}} & i\epsilon_n + \xi_{\mathbf{k}}^d \end{pmatrix} \quad (5)$$

the inverse free propagator. Here $\xi_{\mathbf{k}}^{f(d)} \equiv \epsilon_{\mathbf{k}}^{f(d)} - \mu$, and $k = (\epsilon_n, \mathbf{k})$ is the four-momentum with fermionic Matsubara frequencies $\epsilon_n = (2n+1)\pi T$. Finally,

$$\Delta_x = \begin{pmatrix} 0 & 0 & 0 & -\Delta_x \\ 0 & 0 & \Delta_x & 0 \\ 0 & \bar{\Delta}_x & 0 & 0 \\ -\bar{\Delta}_x & 0 & 0 & 0 \end{pmatrix}, \quad (6)$$

with $x = (\tau, \mathbf{x})$ the conjugate four-coordinate. As already mentioned above, we notice that in a band representation the order parameter Eq. (6) describes both inter- and intraband pairing. That is, changing to a basis that diagonalizes Eq. (5), the homogeneous and static order parameter becomes the Nambu space matrix $\Delta_0 = \begin{pmatrix} 0 & \Delta \\ \Delta & 0 \end{pmatrix}$, with

$$\Delta = \Delta_0 \times \begin{pmatrix} i \sin(2\phi_{\mathbf{k}}) & -\cos(2\phi_{\mathbf{k}}) \\ \cos(2\phi_{\mathbf{k}}) & -i \sin(2\phi_{\mathbf{k}}) \end{pmatrix}, \quad (7)$$

and correspondingly for $\bar{\Delta}$. Here and in the following $\cos(2\phi_{\mathbf{k}}) = \delta \epsilon_{\mathbf{k}} / \Lambda_{\mathbf{k}}$ and $i \sin(2\phi_{\mathbf{k}}) = V_{\mathbf{k}} / \Lambda_{\mathbf{k}}$, with $\epsilon_{\mathbf{k}} = \mathbf{k}^2/(2m)$ and $\Lambda_{\mathbf{k}} = \sqrt{\delta^2 \epsilon_{\mathbf{k}}^2 + |V_{\mathbf{k}}|^2}$. We further notice that Eq. (7) in the limit of equal masses, $m_f = m_d$, reduces to a model with only intraband pairing. The mass difference δ can, therefore, be understood to tune the contribution of interband pairs in the band representation. We next discuss the mean-field properties of the effective action Eq. (4).

III. MEAN-FIELD ANALYSIS

Concentrating on homogeneous configurations, $\Delta(x) = \Delta_0$, the mean-field equation takes the form

$$\frac{1}{g} = \frac{1}{2} \sum_{\mathbf{k}, \eta=\pm} \frac{1}{\epsilon_{\mathbf{k}}^{\eta}} \frac{(\epsilon_{\mathbf{k}}^{\eta})^2 - A_{\mathbf{k}}^+}{(\epsilon_{\mathbf{k}}^{\eta})^2 - (\epsilon_{\mathbf{k}}^{-\eta})^2} \tanh\left(\frac{\epsilon_{\mathbf{k}}^{\eta}}{2T}\right), \quad (8)$$

where here and in the following $A_{\mathbf{k}}^{\pm} = \xi_{\mathbf{k}}^2 + \Delta_0^2 - \delta^2 \epsilon_{\mathbf{k}}^2 \pm |V_{\mathbf{k}}|^2$, and the excitation energies are given by

$$\epsilon_{\mathbf{k}}^{\pm} = \sqrt{\xi_{\mathbf{k}}^2 + |V_{\mathbf{k}}|^2 + \delta^2 \epsilon_{\mathbf{k}}^2 + \Delta_0^2} \pm 2E_{\mathbf{k}}, \quad (9)$$

with $E_{\mathbf{k}} = \sqrt{(\xi_{\mathbf{k}}^2 + \Delta_0^2)\delta^2 \epsilon_{\mathbf{k}}^2 + \xi_{\mathbf{k}}^2 |V_{\mathbf{k}}|^2}$, and we introduced $\xi_{\mathbf{k}} \equiv (\xi_{\mathbf{k}}^d + \xi_{\mathbf{k}}^f)/2 = \epsilon_{\mathbf{k}} - \mu$ (see Appendix B for details).

The ultraviolet divergence in Eq. (8) is accounted for in the standard way [27,52]. That is, substituting the bare interaction parameter for the s -wave scattering length of the two-body problem in vacuum, a_s , and a counter term that regularizes the asymptotic behavior of the sum over momenta, $g^{-1} \mapsto$

$-m/(4\pi a_s) + \sum_{\mathbf{k}} (2\epsilon_{\mathbf{k}})^{-1}$. The interaction is then characterized by the ratio of the average interparticle distance and scattering length, $(k_F a_s)^{-1}$, and varies from large negative values in the weak to large positive values in the strong coupling regime.

A closed set of equations that fixes the chemical potential and order parameter, respectively, critical temperature, is obtained from adding the occupation number equation, $n(T) = T \partial_{\mu} \ln Z$, with $Z = \int \mathcal{D}\Delta e^{-S[\Delta]}$ the partition function resulting from action (4). In our two-band scenario the latter takes the form (see Appendix B for details)

$$n(T) = \sum_{\mathbf{k}, \eta=\pm} \left[1 - \frac{2\xi_{\mathbf{k}}}{\epsilon_{\mathbf{k}}^{\eta}} \frac{(\epsilon_{\mathbf{k}}^{\eta})^2 + A_{\mathbf{k}}^-}{(\epsilon_{\mathbf{k}}^{\eta})^2 - (\epsilon_{\mathbf{k}}^{-\eta})^2} \tanh\left(\frac{\epsilon_{\mathbf{k}}^{\eta}}{2T}\right) \right]. \quad (10)$$

Finally, to eliminate the particle density from the equations, we use that at zero temperature $n(0) = 2F_{\delta}[k_F/(2\pi)]^3$, where the factor 2 here accounts for spin polarizations, and

$$F_{\delta} = \frac{4\pi}{3} \left[\frac{1}{(1+\delta)^{3/2}} + \frac{1}{(1-\delta)^{3/2}} \right]. \quad (11)$$

We notice that the divergence of F_{δ} for $\delta \rightarrow 1$ reflects the diverging density of states (DoS) in the flat band limit $1/m_f \rightarrow 0$. Next, we discuss numerical solutions of the coupled equations (8) and (10) in the zero temperature limit and for temperatures close to the superconducting transition.

A. Numerical solutions at $T = 0$

Taking the continuum limit we arrive at the coupled mean-field equations in the zero temperature limit,

$$\frac{4\pi^2}{k_F a_s} = \int \frac{d^3k}{mk_F} \left[\frac{1}{\epsilon_{\mathbf{k}}} - \frac{1}{\epsilon_{\mathbf{k}}^+ + \epsilon_{\mathbf{k}}^-} \left(1 + \frac{A_{\mathbf{k}}^+}{\sqrt{C_{\mathbf{k}}}} \right) \right], \quad (12)$$

$$F_{\delta} = \int \frac{d^3k}{k_F^3} \left[1 - \frac{\xi_{\mathbf{k}}}{\epsilon_{\mathbf{k}}^+ + \epsilon_{\mathbf{k}}^-} \left(1 + \frac{A_{\mathbf{k}}^-}{\sqrt{C_{\mathbf{k}}}} \right) \right], \quad (13)$$

with $C_{\mathbf{k}} = (A_{\mathbf{k}}^-)^2 + 4|V_{\mathbf{k}}|^2 \Delta_0^2$, which are next solved numerically. We first notice that the anisotropy can be absorbed into a rescaling of the hybridization [53] $\alpha \mapsto \alpha_{\gamma} \equiv \alpha \sqrt{(2 + \gamma^2)}$ and are thus left with three relevant parameters. That is, we next compare solutions for different values of the scattering length $(k_F a_s)^{-1}$, hybridization α_{γ} (for simplicity in the following still denoted by α), and mass difference δ . More specifically, we compare the cases in which either the scattering length $(k_F a_s)^{-1}$ or the hybridization α is used as a tuning parameter, while keeping the other and δ fixed.

Figure 2 shows the mean field order parameter and chemical potential as functions of $(k_F a_s)^{-1}$ for two fixed values $\alpha = 0.5, 2.0$, and the three values $\delta = 0.1, 0.5, 0.9$. In all cases we observe the characteristic features of a BCS-BEC crossover. That is, increasing order parameter and decreasing chemical potential as the tuning parameter $(k_F a_s)^{-1}$ is increased. These features are independent of the specific values of δ and α , although details change. Specifically, for weaker hybridization strength, $\alpha = 0.5$, the δ dependence of the mean field order parameter is more pronounced, showing an increasingly sharp crossover from the BCS into the BEC regime. This can be understood from noting that for moderate hybridization, large

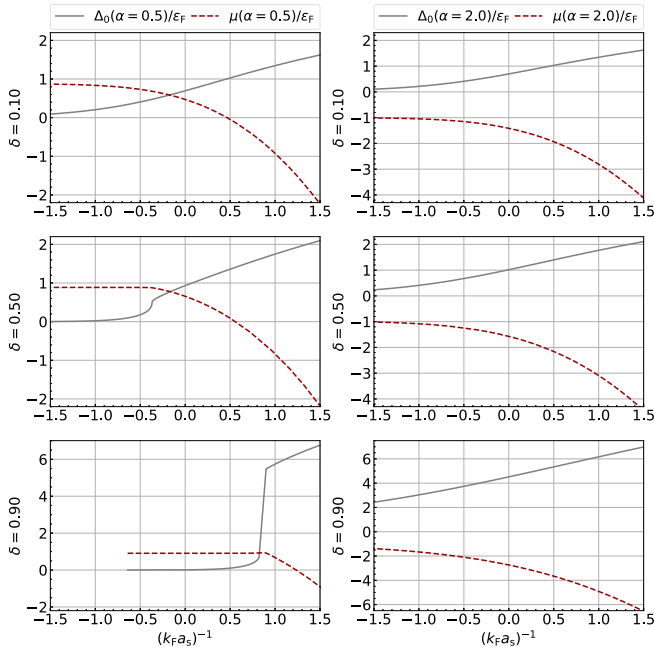


FIG. 2. Zero temperature mean-field order parameter, Δ_0 , and chemical potential, μ , (in units of the Fermi energy) as functions of the scattering length $(k_F a_s)^{-1}$. Here for hybridizations $\alpha = 0.5$ (left), and $\alpha = 2.0$ (right) and mass differences $\delta = 0.1, 0.5, 0.9$.

mass differences kinetically constrain fermions from different bands (and with opposite momenta) to be at a common Fermi level (see also below). Large values δ therefore suppress superconductivity in the BCS regime. In the strong coupling regime, on the other hand, fermions form bound molecules, and increasing δ rather increases the mean field order parameter (see discussion below). This explains the sharp rise of Δ_0 for large mass differences and moderate hybridization. Increasing the hybridization, the kinetic constraint from large mass difference becomes less relevant. Indeed, we observe in the right panels of Fig. 2 that the rapid rises in the mean field order parameter disappears for $\alpha = 2.0$, with Δ_0 increasing approximately linear in $(k_F a_s)^{-1}$ for all values δ .

Finally, we also observe that increasing α at a fixed value $(k_F a_s)^{-1}$ increases Δ_0 , respectively, decreases μ , indicating a transition into strong coupling regime induced by α . To further elaborate on this last point we show in Fig. 3 the mean-field solutions as a function of α for the weak coupling value $(k_F a_s)^{-1} = -0.5$, and for different values $\delta = 0.1, 0.3, 0.7, 0.9$. Increasing α leads to qualitatively the same behavior as in Fig. 2. That is, a decrease in the chemical potential and increase in the order parameter, although for the shown range of α values the latter is visible only for the larger values $\delta = 0.7, 0.9$. For the smaller values $\delta = 0.1, 0.3$, the order parameter varies only by a few percent within the indicated range of α , exhibiting a slightly nonmonotonous α dependence. For the large values of $\delta = 0.7, 0.9$ we see the qualitatively same behavior resulting from either $(k_F a_s)^{-1}$ or α as a tuning parameter. The consequences of an increasing mass difference δ are therefore different in the weak and strong coupling regimes, as already noticed in Fig. 2. That is, Δ_0 in the weak and strong coupling regimes reduces, re-

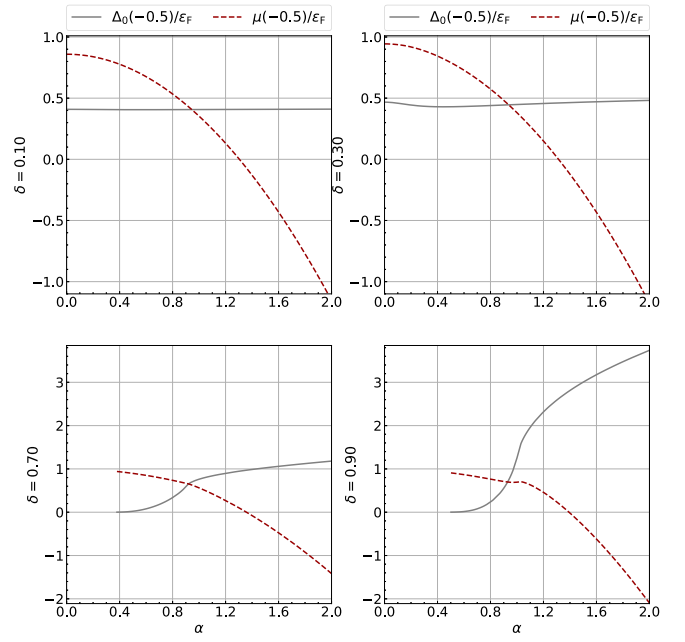


FIG. 3. Zero temperature mean-field order parameter Δ_0 and chemical potential μ (in units of the Fermi energy) as functions of the hybridization strength α . Here for $(k_F a_s)^{-1} = -0.5$ and mass differences $\delta = 0.1, 0.3, 0.7, 0.9$.

spectively, increases with larger values of δ , leading to steeper profiles already mentioned above. The increase of correlations with δ can be related to an increase in the DoS in the flat band limit $1/m_f \rightarrow 0$. Relatedly, we observe that increasing δ , the crossover into the BEC regime occurs for smaller values of the tuning parameters $\alpha, (k_F a_s)^{-1}$. These features are also further investigated below.

Summarizing, the zero temperature mean-field solutions show that odd-parity hybridization plays a similar role as the scattering length. That is, our main observation here is that, analogous to spinor gases, where a tunable BCS-BEC crossover can be induced by controlling spin orbit interaction [39–41], the crossover in the two band superconductors can be driven by increasing the odd-parity hybridization. To further investigate this second scenario we next turn our discussion to finite temperatures.

B. Numerical solutions at $T \simeq T_c$

Close to the phase transition we can neglect Δ_0 in the excitation energies and arrive at the coupled mean field equations,

$$\frac{4\pi^2}{k_F a_s} = \sum_{\eta=\pm} \int \frac{d^3k}{2mk_F} \left[\frac{1}{\epsilon_{\mathbf{k}}} - \frac{1+f_{\mathbf{k}}^{\eta}}{2\xi_{\mathbf{k}}} \tanh\left(\frac{\xi_{\mathbf{k}}^{\eta}}{2T_c}\right) \right], \quad (14)$$

$$F_{\delta} = \sum_{\eta=\pm} \int \frac{d^3k}{2k_F^3} \left[1 - \tanh\left(\frac{\xi_{\mathbf{k}}^{\eta}}{2T_c}\right) \right], \quad (15)$$

with gapless energies $\xi_{\mathbf{k}}^{\pm} = \xi_{\mathbf{k}} \pm \Lambda_{\mathbf{k}}$, and $f_{\mathbf{k}}^{\pm} = \mp |V_{\mathbf{k}}|^2 / (\Lambda_{\mathbf{k}} \xi_{\mathbf{k}}^{\pm})$. The numerical solutions for mean-field parameters μ, T_c as functions of $\alpha, (k_F a_s)^{-1}$, and for different values δ resulting from Eqs. (14) and (15) are shown in Figs. 4 and 5. The results are qualitatively similar for both

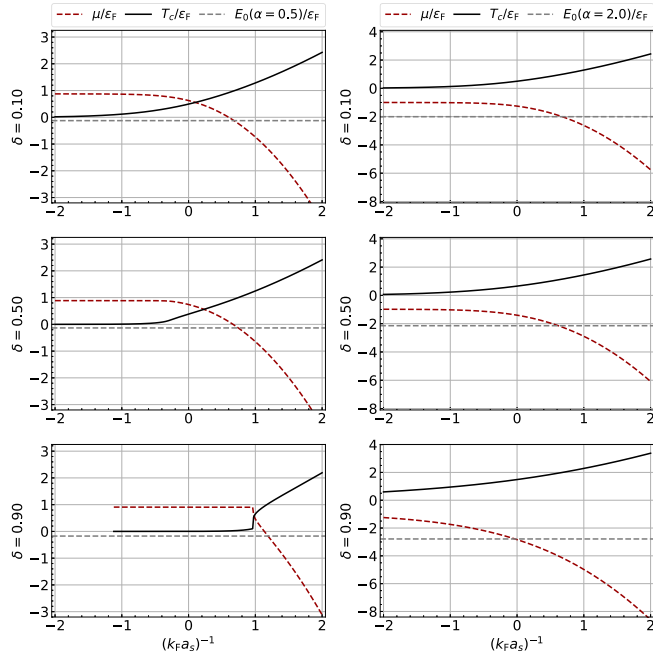


FIG. 4. Finite temperature mean-field critical temperature T_c and chemical potential μ (in units of the Fermi energy) as functions of the scattering length $(k_F a_s)^{-1}$. Here for hybridizations $\alpha = 0.5$ (left) and $\alpha = 2.0$ (right), and mass differences $\delta = 0.1, 0.5, 0.9$. The gray dashed line indicates the band bottom E_0 .

tuning parameters, and also similar to the behavior of μ , Δ_0 in the zero temperature limit. That is, we again observe the characteristic features of a BCS-BEC crossover, viz. increasing critical temperature and decreasing chemical potential as the tuning parameter is increased. To identify the crossover into the strong coupling regime, we indicate in all figures the energy of the band minimum in the absence of pairing, E_0 , by dashed gray lines.

Figure 4 shows the critical temperature and chemical potential as functions of $(k_F a_s)^{-1}$, for hybridization strengths $\alpha = 0.5$ (left) and $\alpha = 2.0$ (right) and mass differences $\delta = 0.1, 0.5, 0.9$. As already mentioned, the crossover into the strong coupling regime (indicated by the crossing $E_0 \simeq \mu$) is shifted to smaller values of $(k_F a_s)^{-1}$ as either α or δ is increased. Again we observe that for the smaller value $\alpha = 0.5$ the crossover becomes more pronounced as δ increases. Figure 5 shows the corresponding behavior of the critical temperature (main panel) and chemical potential (inset) as α is varied, here for a scattering length $(k_F a_s)^{-1} = -0.5$ in the weak coupling regime, and for mass differences $\delta = 0.1, 0.3, 0.7, 0.9$. Similar to the order parameter in the zero-temperature limit, we find for small mass differences δ a weak α dependence of T_c in the indicated range of α values, which then becomes more pronounced as δ increases. That is, T_c decreases, respectively, increases in the weak and strong coupling regimes as δ increases. Interestingly, $T_c(\alpha)$ appears to intersect in a single point $\alpha \simeq \alpha_0$ for different δ values, indicating some form of scaling that is not understood at the moment (see Appendix E for further details). The inset shows the α dependence of the chemical potential for the corresponding values of $(k_F a_s)^{-1}$ and δ . Notice that for the range

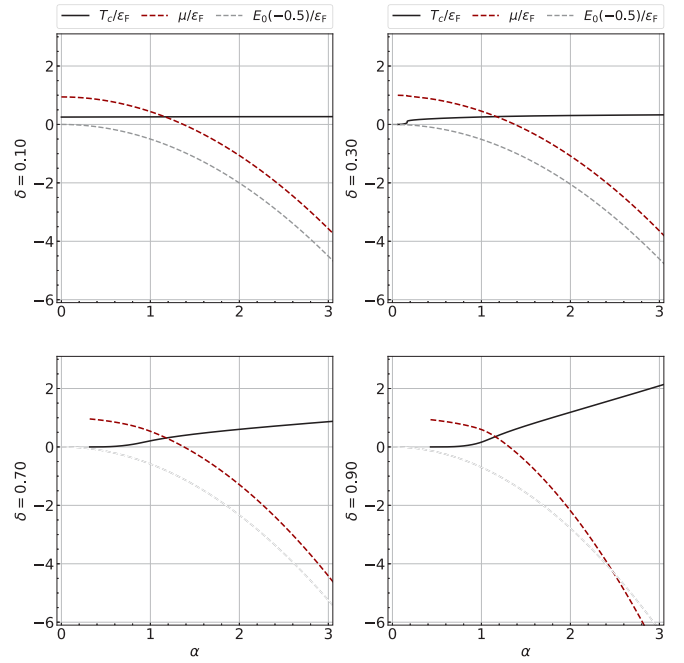


FIG. 5. Main: Finite temperature mean-field critical temperature T_c (in units of the Fermi energy) as functions of α . Here for scattering lengths $(k_F a_s)^{-1} = -0.5$ in the weak coupling regime, and mass differences $\delta = 0.1, 0.3, 0.7, 0.9$. Inset: Chemical potential μ (in units of the Fermi energy) as functions of α , and the same set of parameters. The gray dashed line indicates the band bottom E_0 , and the crossover from the BCS to the BEC regime occurs when $\mu \simeq E_0$ (here only for the largest value of mass difference $\delta = 0.9$).

of α values presented, μ intersects E_0 only for the largest value $\delta = 0.9$. As δ decreases, larger α values are required for the BCS-BEC crossover to take place. At the same time, increasing the scattering length the crossover occurs for smaller values α (see also Fig. 7 below). The α -driven BCS-BEC crossover is thus favored in systems with one dispersive and one flat band, as typically encountered in the heavy fermion systems with a shallow band of f electrons and a wide band of d electrons.

Again we observe that the impact of large mass differences δ is qualitatively different in the weak and strong coupling regimes. To illustrate this further, we show in Fig. 6 the δ dependence of the critical temperature (left) and chemical potential (right) for three different values $(k_F a_s)^{-1} = \pm 0.5, 0$ and $\alpha = 0.5$ (top) and 2.0 (bottom). One clearly sees the opposite impact of an increasing δ in the weak and strong coupling regimes. That is, a decreasing (eventually dropping to zero) and increasing critical temperature in the weak (top) and strong coupling (bottom) regimes, respectively, accompanied by an increasing, respectively, decreasing chemical potential. Notice that for large hybridization the chemical potential eventual drops below the band bottom E_0 (indicated by the dashed gray line) as δ is increased.

To summarize the main observation of this section, we confirm that the relevant scale for the hybridization driven BCS-BEC crossover depends strongly on the ratio of effective masses. Large mass differences in the weak coupling regime suppress superconductivity, and the weak coupling

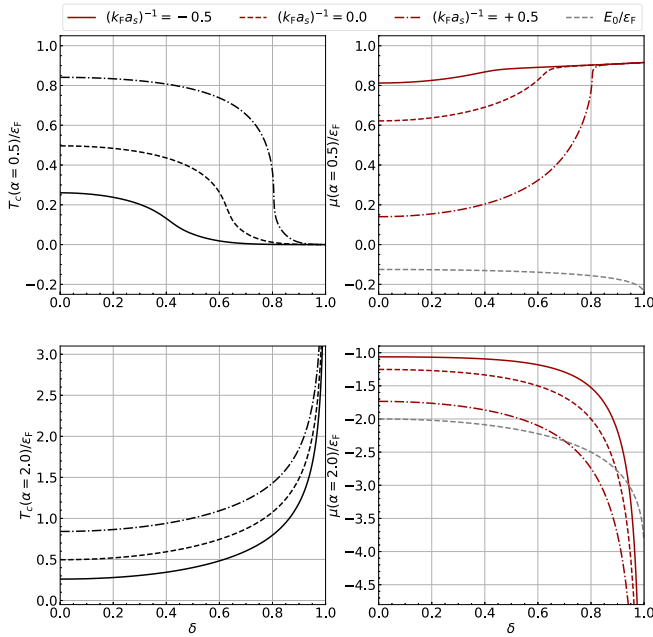


FIG. 6. Finite temperature mean-field critical temperature, T_c , (left) and chemical potential, μ , (right) as functions of the mass difference δ (the grey dashed line again denotes the band bottom E_0). Here for three values of the scattering length $(k_F a_s)^{-1} = \pm 0.5, 0$, and hybridizations $\alpha = 0.5$ (top) and $\alpha = 2.0$ (bottom).

order parameter, destroyed by δ , can be restored by the hybridization. This is similar to spin orbit coupled gases, where large Zeeman fields destroy superconductivity and can be restored by spin orbit interaction. Indeed, upon substituting the Zeeman and spin orbit interaction energies for $\delta\epsilon_{\mathbf{k}}$ and $V_{\mathbf{k}}$, respectively, we can repeat the argument of Ref. [45]. That is, without hybridization a finite mass difference lifts the degeneracy between electrons from f and d bands and thus destroys pairing when the mass difference exceeds the pairing interaction in units of the Fermi energy. This can be understood from the quasiparticle spectrum Eq. (9), where the excitation gap $E_g = \min_{\mathbf{k}} |\sqrt{\xi_{\mathbf{k}}^2 + \Delta_0^2} - \delta\epsilon_{\mathbf{k}}| = 0$ for a suitable chosen \mathbf{k} when $\alpha = 0$ and $\delta > \Delta_0/\epsilon_F$. With hybridization, on the other hand, the bands of the single particle Hamiltonian both contain f and d components even with a large mass difference, leading to nonzero Cooper pairing between two fermions in the same band with opposite momenta. Finally, the crossover is favored in systems with one dispersive and one flat band, viz. large δ . This is specifically interesting for heavy fermion systems with wide d and shallow f bands.

We observe in Fig. 5 a monotonic growth of T_c with increasing α . A similar (algebraic) growth of the mean-field critical temperature is observed in spinor gases with increasing strength of spin orbit interaction [40]. An (exponential) growth of the critical temperature is also observed for increasing $(k_F a_s)^{-1}$ at fixed α . This monotonic growth of the mean field critical temperature with the tuning parameter is a well-understood artifact of the mean-field analysis of the BCS-BEC crossover. It is also observed in the single band superconductors, where the true critical temperature has a peak at $(k_F a_s)^{-1} \simeq 0$ and saturates to a constant value for strong

couplings. To overcome the artifact of the mean-field analysis in the present case, and to estimate the critical temperature as a function of the hybridization strength in the strong coupling regime, we next turn to the effect of pair fluctuations.

IV. STRONG COUPLING LIMIT

In the strong coupling regime, the mean field critical temperature T_c rather describes the dissociation energy of pairs than the temperature scale at which coherence is established [54]. To overcome the deficiency of the bare mean-field analysis, and to capture the critical temperature at strong couplings, it is sufficient to account for pair fluctuations in a one-loop approximation.

A. Gaussian pair fluctuations

Relying then on a one loop approximation, we expand the effective action Eq. (4) in gaussian fluctuations of the order parameter. The calculation is simplified in a basis diagonalizing the free Green's function and results in the effective action for pair fluctuations (see Appendix C for details),

$$S^{(2)}[\Delta] = \sum_q \Gamma_q^{-1} |\Delta_q|^2, \quad (16)$$

with the vertex function,

$$\Gamma_q^{-1} = \frac{2}{g} - \sum_{\mathbf{k}, \eta, \bar{\eta}} F_{\mathbf{k}, \mathbf{q}}^{\eta \bar{\eta}} \frac{1 - n_F(\xi_{\mathbf{k}-\mathbf{q}/2}^{\eta}) - n_F(\xi_{\mathbf{k}+\mathbf{q}/2}^{\bar{\eta}})}{i\omega_m + \xi_{\mathbf{k}-\mathbf{q}/2}^{\eta} + \xi_{\mathbf{k}+\mathbf{q}/2}^{\bar{\eta}}}. \quad (17)$$

Here n_F is the Fermi distribution,

$$F_{\mathbf{k}, \mathbf{q}}^{\eta \bar{\eta}} = \begin{cases} \cos^2(\phi_{\mathbf{k}-\mathbf{q}/2} + \phi_{\mathbf{k}+\mathbf{q}/2}) & \eta \neq \bar{\eta}, \\ \sin^2(\phi_{\mathbf{k}-\mathbf{q}/2} + \phi_{\mathbf{k}+\mathbf{q}/2}) & \eta = \bar{\eta}, \end{cases} \quad (18)$$

and for convenience of the reader we recall that $i \sin(2\phi_{\mathbf{k}}) = V_{\mathbf{k}}/\Lambda_{\mathbf{k}}$ and $\cos(2\phi_{\mathbf{k}}) = \delta\epsilon_{\mathbf{k}}/\Lambda_{\mathbf{k}}$. The vertex function, Eq. (17), holds the relevant information on pair fluctuations, and gaussian integration over Δ leads to a spectral determinant which includes the effect of pair fluctuations into the number equation. The resulting coupled mean-field equations in the two-band scenario become rather involved, and we here focus on the strong coupling regime, where the chemical potential is always below the band minimum E_0 , and fermionic occupations are (exponentially) small. Neglecting then contributions from Fermi distribution functions, we perform a gradient expansion in small momenta and frequencies to arrive at $\Gamma_q^{-1} \simeq M_0 + \frac{J_0}{2}(i\omega_m + \frac{\mathbf{q}^2}{4m}) - \delta^2 \Omega_{\mathbf{q}}$, where

$$\begin{aligned} M_0 &= \pi v_0 \left(\sqrt{x_{\mu}} - \frac{1}{k_F a_s} \right) - \sum_{\mathbf{k}} \frac{\Theta_{\mathbf{k}}}{\xi_{\mathbf{k}}}, \\ J_0 &= \frac{\pi v_0}{2\epsilon_F \sqrt{x_{\mu}}} + \sum_{\mathbf{k}} \Theta_{\mathbf{k}} \left(\frac{1}{\xi_{\mathbf{k}}^2} + \frac{2}{\xi_{\mathbf{k}}^2 - \Lambda_{\mathbf{k}}^2} \right), \\ \Omega_{\mathbf{q}} &= \frac{\mathbf{q}^2}{4m} \sum_{\mathbf{k}} \frac{\epsilon_{\mathbf{k}}}{\xi_{\mathbf{k}}} \frac{\Theta_{\mathbf{k}}}{\xi_{\mathbf{k}}^2 - \Lambda_{\mathbf{k}}^2} \\ &\quad + \sum_{\mathbf{k}} \frac{1}{\xi_{\mathbf{k}}^3} \left[\left(\frac{\mathbf{k} \cdot \mathbf{q}}{2m} \right) (1 + \Theta_{\mathbf{k}}) - \frac{\epsilon_{\mathbf{k}} V_{\mathbf{q}}}{\xi_{\mathbf{k}}^2 - \Lambda_{\mathbf{k}}^2} \right]^2, \end{aligned} \quad (19)$$

with v_0 the DoS at the Fermi level, and we defined $x_\mu \equiv |\mu|/\epsilon_F$ and $\Theta_{\mathbf{k}} \equiv \frac{|V_{\mathbf{k}}|^2}{\xi_{\mathbf{k}}^2 - \Lambda_{\mathbf{k}}^2}$. Notice that, although not explicitly stated, all of the above expressions depend on $(k_F a_s)^{-1}$, α , and δ .

B. Critical temperature

We can now deduce the critical temperature T_c in the BEC regime from the dispersion relation of the pair propagator. To this end we notice that, incorporating an overall constant into the fields, Eq. (16) can be rewritten as

$$S^{(2)}[\bar{\Delta}, \Delta] = \sum_q \bar{\Delta}_q (i\omega_m + \epsilon_{\mathbf{q}} + \mu_{\text{eff}}) \Delta_q, \quad (20)$$

with $\mu_{\text{eff}} = 2\epsilon_F M_0 / (\pi v_0 J_0)$, and the dispersion $\epsilon_{\mathbf{q}} = \sum_{i=1}^3 (\delta_{ij} - \frac{2\delta^2}{J_0} \Lambda_{ij}) \frac{q_i q_j}{4m}$, where Λ a symmetric block-diagonal matrix reflecting tetragonal symmetry,

$$\Lambda_{xx} = \sum_{\mathbf{k}} \left[\frac{\epsilon_{\mathbf{k}}}{\xi_{\mathbf{k}} \xi_{\mathbf{k}}^2 - \Lambda_{\mathbf{k}}^2} + \frac{k_x^2}{2m} \frac{(1 + \Theta_{\mathbf{k}})^2}{\xi_{\mathbf{k}}^3} \right], \quad (21)$$

$$\Lambda_{yy} = \sum_{\mathbf{k}} \left[\frac{\epsilon_{\mathbf{k}}}{\xi_{\mathbf{k}} \xi_{\mathbf{k}}^2 - \Lambda_{\mathbf{k}}^2} + \frac{k_y^2}{2m} \frac{(1 + \Theta_{\mathbf{k}})^2}{\xi_{\mathbf{k}}^3} \right], \quad (22)$$

$$\Lambda_{zz} = \sum_{\mathbf{k}} \left[\frac{\epsilon_{\mathbf{k}}}{\xi_{\mathbf{k}} \xi_{\mathbf{k}}^2 - \Lambda_{\mathbf{k}}^2} + \frac{k_z^2}{2m} \frac{(1 + \Theta_{\mathbf{k}})^2}{\xi_{\mathbf{k}}^3} - \frac{2\epsilon_{\mathbf{k}} \Theta_{\mathbf{k}} (1 + \Theta_{\mathbf{k}})}{\xi_{\mathbf{k}}^3} + \alpha^2 \epsilon_F \frac{\epsilon_{\mathbf{k}}^2}{\xi_{\mathbf{k}}^3} \frac{\Theta_{\mathbf{k}}}{\xi_{\mathbf{k}}^2 - \Lambda_{\mathbf{k}}^2} \right], \quad (23)$$

with $\Lambda_{xx} = \Lambda_{yy}$, while the remaining off-diagonal components are zero.

Using then the standard relation for weakly interacting Bose gases [55] between critical temperature, bosonic density $n/2$, and effective masses we can relate T_c in the strong coupling regime to the scattering length $(k_F a_s)^{-1}$, hybridization α , and mass difference δ . That is,

$$T_c = \frac{\pi}{(m_x m_y m_z)^{1/3}} \left[\frac{n}{2\zeta(3/2)} \right]^{2/3}, \quad (24)$$

where $m_i = m/(1 - 2\delta^2 \Lambda_{ii}/J_0)$, and the appearance of anisotropic masses is another common characteristic with the spin-orbit coupled systems [40]. Figure 7 shows the critical temperature as a function of α for two different values $(k_F a_s)^{-1} = 0.1$ (left) and 0.5 (right), and $\delta = 0.7$ (top) and 0.9 (bottom). The mean-field result, applicable in the weak coupling regime, is indicated by the blue dashed lines. The result Eq. (24), describing the strong coupling regime, is shown by the black dashed-dotted line. We here assumed that in the strong coupling limit the boson density is half of the total fermion density. The crossover region where $E_0 = \mu$ is indicated by the vertical dotted line. For large hybridization, the critical temperature in the strong coupling regime saturates to a value that in general depends on both $(k_F a_s)^{-1}$ and δ . For $\delta = 0$, expression simplifies to that of a gas of bosons with mass $2m$ and density $n/2 = k_F^3/(3\pi^2)$, and $T_c(\delta \rightarrow 0) \simeq 0.35\epsilon_F$. That is, independent of α , and $(k_F a_s)^{-1}$, as long as the latter are within the strong coupling regime. (Notice, however, that for $\delta = 0$ we could only establish superconducting mean-

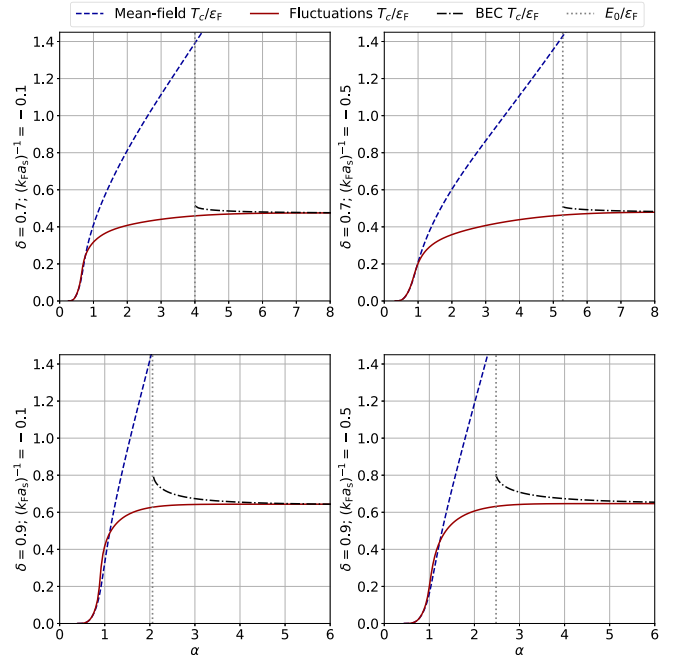


FIG. 7. Critical temperature as a function of hybridization strength α , for scattering length $(k_F a_s)^{-1} = -0.1$ (left) and -0.5 (right), and $\delta = 0.7$ (top) and 0.9 (bottom). The blue dashed and black dash-dotted lines are the analytical predictions for the weak and strong coupling regimes, respectively. The vertical dotted lines indicate the values at which the chemical potential passes the band bottom $E_0 \simeq \mu$. The solid line shows the interpolation discussed in the main text.

field solutions for large scattering lengths). This value is a factor $z^{2/3}$ larger than the corresponding value, $T_c \simeq 0.22\epsilon_F$, for single-band superconductors, where $z = 2$ the number of bands. As seen from Fig. 7, the critical temperature [here for scattering lengths $(k_F a_s)^{-1} = -0.1$ and -0.5] then increases for larger δ , taking the value $T_c \simeq 0.48\epsilon_F$ for $\delta = 0.7$, and nearly doubles to $T_c \simeq 0.65\epsilon_F$ for $\delta = 0.9$. The entire profile interpolating between both curves can be numerically found from including the pair susceptibility into the mean-field equation which is beyond the scope of the present work. For a rough estimate, we follow Refs. [40,42] and interpolate the weak and strong coupling regimes by adding the fluctuation contribution, $n_{\text{fluc}} = \sum_{\mathbf{q}} 1/(e^{\sum_i q_i^2/(4m_i T_c)} - 1)$, to the right hand side of the number equation (10), where m_i are the effective masses defined previously. Finally the interpolations shown as solid red lines in Fig. 7 successfully reproduce the critical temperatures at both weak and strong coupling regimes.

V. DISCUSSION

We have studied the effect of an odd-parity hybridization on the BCS-BEC crossover in multi-orbital superconductors. Our analysis is motivated by superconductors with orbitals of opposite parity coexisting at a common Fermi surface, such as heavy fermion superconductors, and builds on the two-band model previously introduced by Khomskii *et al.* [22,23] to study thermodynamic properties of the latter. Specifically, we

have shown that the odd-parity hybridization can play a similar role as the scattering length, driving the crossover from the weak coupling BCS state to BEC at strong coupling. We found that the relevant scale for the crossover depends on the ratio of effective masses and is favored in systems with a narrow and a wide band, as typically encountered in heavy fermion systems with their localized f and delocalized d electrons. We also found that large mass differences have opposite impacts in the weak and strong coupling regimes. That is, reducing interband pairing at weak couplings and enhancing pairing in the strong coupling regime. We related the enhancement of strong correlations to the diverging DoS in the flat band limit $1/m_f \rightarrow 0$, while the suppression of superconductivity in the weak coupling limit can be understood from the kinetic constraints for pairing of fermions from different bands and with opposite momenta induced by large δ . The suppression of superconductivity in the weak coupling regime at moderated hybridization and large mass differences is thus restored by increasing hybridization. This is similar to spin orbit coupled gases, where large Zeeman fields destroy superconductivity and can be restored by spin orbit interaction [45]. Relatedly, the sharp profile of the mean field order parameter as a function of the scattering length at large mass differences disappears with increasing hybridization.

We conclude with several comments on the model and future directions. Our analysis builds on a simple model by Khomskii and co-workers, and it should be interesting to study extensions to more sophisticated models. The dispersions of free electrons, considered here, left the mass difference δ as the only relevant parameter from the band structure. As discussed above, δ plays an important role in the α -driven BCS-BEC crossover, and it should be interesting to see how additional parameters resulting from more realistic band structures affect the latter. Also, the present model only accounts for pairs of f and d electrons, and pairing in the s -wave channel. In the presence of finite hybridizations this includes both intra- and interband pairs, as can be seen in the more physical band representation, with the density of interband pairs proportional to δ . More specifically, tuning δ one interpolates between a scenario of pure intraband pairing to one with both intra- and interband pairs in the band representation. Still, one may wonder how inclusion of pairing in the d or f band changes the discussed results. We first notice that the latter add a pairing potential in the band representation similar to Eq. (7), where now the intraband contribution is determined by δ and the interband contribution is proportional to the hybridization. We further show in Appendix D that in a model with only intraband pairing increasing α does not tune the system into a strong coupling regime. We, therefore, expect that in a model with pairing of both f and d electrons, and the f - d pairs considered here, the latter will dominate with increasing hybridization. Based on these observations, we expect that the α -driven BCS-BEC crossover also applies to more complex situations, however, more detailed studies are required to corroborate this picture. In the same way, it should be interesting to include the possibility of different pairing symmetries into the two band systems with finite hybridization.

Finally, our results are derived from a mean-field analysis in the weak coupling regime, and in the strong coupling

regime the effect of pair fluctuations is included in a one-loop approximation. We here focused on the weak and strong coupling regimes and resorted to a simple interpolation in between. Results for the entire crossover can be numerically found by including the pair susceptibility, derived in Sec. IV, into the coupled mean field equations for the critical temperature and chemical potential. Solving the rather involved coupled equations is, however, numerically challenging and beyond the scope of the present work.

ACKNOWLEDGMENT

We acknowledge financial support by Brazilian agencies CAPES, CNPq, and FAPERJ.

APPENDIX A: EFFECTIVE ACTION

Within the path integral formalism our action is expressed through the Grassmann fields $\psi_{k\sigma}^{d(f)}$ as

$$S[\psi] = \sum_{k,\sigma,l} \bar{\psi}_{k\sigma}^l (\xi_{\mathbf{k}}^l - i\epsilon_n) \psi_{k\sigma}^l - \frac{g}{2} \sum_{k,\bar{k},q,\sigma} \bar{\psi}_{k+q\sigma}^f \bar{\psi}_{-k-\sigma}^d \psi_{-\bar{k}+q-\sigma}^d \psi_{k\sigma}^f + \sum_{k,\sigma} (V_{\mathbf{k}} \bar{\psi}_{k\sigma}^f \psi_{k\sigma}^d + \bar{V}_{\mathbf{k}} \bar{\psi}_{k\sigma}^d \psi_{k\sigma}^f). \quad (\text{A1})$$

We decouple the quartic term in the Cooper channel to arrive at the partition function $\mathcal{Z} = \int \mathcal{D}[\psi] \mathcal{D}[\Delta] e^{-S[\psi,\Delta]}$, with action,

$$S[\psi, \Delta] = \sum_q \frac{2}{g} |\Delta_q|^2 + \sum_{k,\sigma,l} \bar{\psi}_{k\sigma}^l (\xi_{\mathbf{k}}^l - i\epsilon_n) \psi_{k\sigma}^l - \sum_{k,q,\sigma} (\Delta_q \bar{\psi}_{k+q\sigma}^f \bar{\psi}_{-k-\sigma}^d + \bar{\Delta}_q \psi_{-k-\sigma}^d \psi_{k+q\sigma}^f) + \sum_{k,\sigma} (V_{\mathbf{k}} \bar{\psi}_{k\sigma}^f \psi_{k\sigma}^d + \bar{V}_{\mathbf{k}} \bar{\psi}_{k\sigma}^d \psi_{k\sigma}^f). \quad (\text{A2})$$

Introducing the Nambu spinor representation $\bar{\Psi}_k = (\bar{\psi}_{k\uparrow}^f, \bar{\psi}_{k\uparrow}^d, \psi_{-k\downarrow}^f, \psi_{-k\downarrow}^d)$ the action can be expressed as

$$S[\Psi, \Delta] = \sum_q \left(\frac{2}{g} |\Delta_q|^2 - \sum_k \bar{\Psi}_{k+q} \mathbf{G}_{\Delta}^{-1} \Psi_{k-q} \right) + C, \quad (\text{A3})$$

with \mathbf{G}_{Δ}^{-1} defined in Eqs. (5) and (6) in the main text, and the constant $C = \sum_{l=f,d} \sum_{\mathbf{k}} \xi_{\mathbf{k}}^l / T$ is due to reorganization of fermionic operators in the Nambu representation. Upon integration over fermionic fields we finally arrive at

$$S[\Delta] = \sum_q \left(\frac{2}{g} |\Delta_q|^2 - \ln \text{Det } \mathbf{G}_{\Delta}^{-1} \right) + C, \quad (\text{A4})$$

which, using the identity $\ln \text{Det } \mathbf{G}_{\Delta}^{-1} = \text{Tr} \ln \mathbf{G}_{\Delta}^{-1}$, becomes Eq. (4) in the main text.

APPENDIX B: MEAN-FIELD EQUATIONS

Concentrating on a static and homogeneous order parameter, $\Delta_q = \Delta_0$, variation of the action $\delta_\Delta S = 0$ results in

$$\frac{2\bar{\Delta}}{g} - \text{Tr}(\mathbf{G}\delta_\Delta \mathbf{G}^{-1}) = 0. \quad (\text{B1})$$

The only nonzero components are $(\delta_\Delta \mathbf{G}^{-1})_{23} = 1$ and $(\delta_\Delta \mathbf{G}^{-1})_{14} = -1$, and therefore $\text{Tr}(\mathbf{G}\delta_\Delta \mathbf{G}^{-1}) = T \sum_k (\mathbf{G}_{32} - \mathbf{G}_{41})$. The procedure to obtain the relevant \mathbf{G} components is straightforward but tedious. Skipping then longer algebraic manipulations and assuming an s -wave order parameter, $\Delta_0 = \bar{\Delta}_0$, the saddle-point equation takes the form

$$\frac{2}{g} = 2T \sum_{\mathbf{k}, \epsilon_n} \frac{\epsilon_n^2 + \xi_{\mathbf{k}}^f \xi_{\mathbf{k}}^d + |\mathbf{V}_{\mathbf{k}}|^2 + \Delta_0^2}{\text{Det} \mathbf{G}^{-1}}, \quad (\text{B2})$$

with $\text{Det} \mathbf{G}^{-1} = \epsilon_n^4 + 2B_{\mathbf{k}} \epsilon_n^2 + C_{\mathbf{k}}$, where

$$B_{\mathbf{k}} = \xi_{\mathbf{k}}^2 + \delta^2 \epsilon_{\mathbf{k}}^2 + \Delta_0^2 + |\mathbf{V}_{\mathbf{k}}|^2, \quad (\text{B3})$$

$$C_{\mathbf{k}} = (A_{\mathbf{k}}^-)^2 + 4|\mathbf{V}_{\mathbf{k}}|^2 \Delta_0^2, \quad (\text{B4})$$

and we introduced $\xi_{\mathbf{k}} \equiv (\xi_{\mathbf{k}}^d + \xi_{\mathbf{k}}^f)/2 = \epsilon_{\mathbf{k}} - \mu$. Performing the sum over the odd frequencies ϵ_n we finally arrive at Eq. (8).

Similarly, we can derive the occupation number equation starting out from $n(T) = T \partial_\mu \ln Z$, where $Z = \int \mathcal{D}\Delta e^{-S[\Delta]}$ the partition function. Inserting action Eq. (A4), we arrive at

$$n(T) = \sum_{\mathbf{k}} \left(2 + T \frac{\partial}{\partial \mu} \sum_{\epsilon_n} \ln \det \mathbf{G}^{-1} \right), \quad (\text{B5})$$

where the first contribution derives from the constant $\partial_\mu C$. More explicitly,

$$n(T) = \sum_{\mathbf{k}} \left(2 + T \sum_{\epsilon_n} \frac{2\partial_\mu B_{\mathbf{k}} \epsilon_n^2 + \partial_\mu C_{\mathbf{k}}}{\epsilon_n^4 + 2B_{\mathbf{k}} \epsilon_n^2 + C_{\mathbf{k}}} \right), \quad (\text{B6})$$

and with the definitions given in Eq. (B3)

$$\partial_\mu B_{\mathbf{k}} = -2\xi_{\mathbf{k}}, \quad \partial_\mu C_{\mathbf{k}} = -2\xi_{\mathbf{k}} A_{\mathbf{k}}^-, \quad (\text{B7})$$

we can sum over the Matsubara frequencies in the second term to arrive at Eq. (10) in the main text where we recall that $A_{\mathbf{k}}^\pm = \xi_{\mathbf{k}}^2 - \delta^2 \epsilon_{\mathbf{k}}^2 + \Delta_0^2 \pm |\mathbf{V}_{\mathbf{k}}|^2$.

APPENDIX C: GAUSSIAN PAIR PROPAGATOR

To derive the Gaussian pair propagator, we start out from an expansion of the ‘tr log,’

$$\text{Tr} \ln \mathbf{G}_\Delta^{-1} = \text{Tr} \ln \mathbf{G}_0^{-1} - \sum_{n=1}^{\infty} \frac{1}{2n} \text{Tr}(\mathbf{G}_0 \Delta)^{2n}, \quad (\text{C1})$$

and restrict ourselves to the leading second order contribution $n = 1$. The calculation is then simplified in a rotated basis, i.e., applying a Bogoliubov-de Gennes transformation, $\mathbf{U}_{\mathbf{k}} = \mathbb{1}_2 \otimes \exp(i\sigma_1 \phi_{\mathbf{k}})$, with σ_1 the first Pauli matrix acting in Nambu space which diagonalizes \mathbf{G}_0 . That is,

$$S^{(2)}[\Delta] = \sum_q \left[\frac{2}{g} |\Delta_q|^2 + \frac{1}{2} \text{Tr}(\tilde{\mathbf{G}}_0 \tilde{\Delta})^2 \right], \quad (\text{C2})$$

where

$$\tilde{\mathbf{G}}_0 = \mathbf{U}_{\mathbf{k}}^\dagger \mathbf{G}_0 \mathbf{U}_{\mathbf{k}} = \begin{bmatrix} G_k^- & 0 & 0 & 0 \\ 0 & G_k^+ & 0 & 0 \\ 0 & 0 & -G_{-k}^- & 0 \\ 0 & 0 & 0 & -G_{-k}^+ \end{bmatrix}, \quad (\text{C3})$$

with the \pm quasiparticles Green’s function $G_k^\pm = (i\epsilon_n - \xi_{\mathbf{k}}^\pm)^{-1}$ and the fluctuations matrix

$$\begin{aligned} \tilde{\Delta}(k, q) &= \mathbf{U}_{\mathbf{k}+\mathbf{q}/2}^\dagger \Delta_q \mathbf{U}_{\mathbf{k}-\mathbf{q}/2} \\ &= \cos(\phi_{\mathbf{k}+\mathbf{q}/2} + \phi_{\mathbf{k}-\mathbf{q}/2}) \Delta_c(q) \\ &\quad + i \sin(\phi_{\mathbf{k}+\mathbf{q}/2} + \phi_{\mathbf{k}-\mathbf{q}/2}) \Delta_s(q), \end{aligned} \quad (\text{C4})$$

where

$$\Delta_c(q) = \begin{bmatrix} 0 & 0 & 0 & -\Delta_q \\ 0 & 0 & \Delta_q & 0 \\ 0 & \bar{\Delta}_{-q} & 0 & 0 \\ -\bar{\Delta}_{-q} & 0 & 0 & 0 \end{bmatrix} \quad (\text{C5})$$

and

$$\Delta_s(q) = \begin{bmatrix} 0 & 0 & -\Delta_q & 0 \\ 0 & 0 & 0 & \Delta_q \\ \bar{\Delta}_{-q} & 0 & 0 & 0 \\ 0 & -\bar{\Delta}_{-q} & 0 & 0 \end{bmatrix}, \quad (\text{C6})$$

with $i \sin(2\phi_{\mathbf{k}}) = V_{\mathbf{k}}/\Lambda_{\mathbf{k}}$, and $\cos(2\phi_{\mathbf{k}}) = \delta \epsilon_{\mathbf{k}}/\Lambda_{\mathbf{k}}$. Notice that the hybridization introduces an intraband pairing between \pm bands, Δ_s . Gaussian fluctuations then have the two contributions

$$\sum_q \text{Tr}(\tilde{\mathbf{G}}_0 \tilde{\Delta})^2 = -2T(M_q + N_q) |\Delta_q|^2, \quad (\text{C7})$$

where

$$\begin{aligned} M_{2q} &= \sum_{\mathbf{k}, \epsilon_n} C_{\mathbf{k}\mathbf{q}} (G_{k-q}^+ G_{-k-q}^- + G_{k-q}^- G_{-k-q}^+), \\ N_{2q} &= \sum_{\mathbf{k}, \epsilon_n} S_{\mathbf{k}\mathbf{q}} (G_{k-q}^+ G_{-k-q}^+ + G_{k-q}^- G_{-k-q}^-), \end{aligned} \quad (\text{C8})$$

and $C_{\mathbf{k}\mathbf{q}} = \cos^2(\phi_{\mathbf{k}-\mathbf{q}} + \phi_{\mathbf{k}+\mathbf{q}})$, $S_{\mathbf{k}\mathbf{q}} = \sin^2(\phi_{\mathbf{k}-\mathbf{q}} + \phi_{\mathbf{k}+\mathbf{q}})$. Lastly, performing the summation over fermionic frequencies

$$T \sum_{\epsilon_n} G_{k-q}^\pm G_{-k-q}^\pm = \frac{1 - n_F(\xi_{\mathbf{k}+\mathbf{q}}^\pm) - n_F(\xi_{\mathbf{k}-\mathbf{q}}^\pm)}{i\omega_m + \xi_{\mathbf{k}+\mathbf{q}}^\pm + \xi_{\mathbf{k}-\mathbf{q}}^\pm}, \quad (\text{C9})$$

we arrive at the gaussian effective action $S^{(2)}[\Delta] = \sum_q \Gamma_q^{-1} |\Delta_q|^2$ with the vertex function given in Eq. (17) in the main text.

APPENDIX D: f -BAND PAIRING

For comparison we here discuss the mean-field analysis of the main text for a model with pairing in only one of the bands (here the f band). The mean-field order parameter then reads $\Omega_0 = g \sum_{\mathbf{k}} \langle \hat{f}_{-\mathbf{k}\downarrow} \hat{f}_{\mathbf{k}\uparrow} \rangle$, with g a positive interaction constant in the f band, and proceeding analogously as for the interband pairing, we arrive at the gap equation

$$\frac{m_d}{2\pi a_s} = \sum_{\mathbf{k}} \frac{1}{\epsilon_{\mathbf{k}}^d} - \sum_{\mathbf{k}, \eta=\pm} \frac{1}{\epsilon_{\mathbf{k}}^\eta} \frac{(\epsilon_{\mathbf{k}}^\eta)^2 - (\xi_{\mathbf{k}}^d)^2}{(\epsilon_{\mathbf{k}}^\eta)^2 - (\epsilon_{\mathbf{k}}^{-\eta})^2} \tanh\left(\frac{\epsilon_{\mathbf{k}}^\eta}{2T}\right), \quad (\text{D1})$$

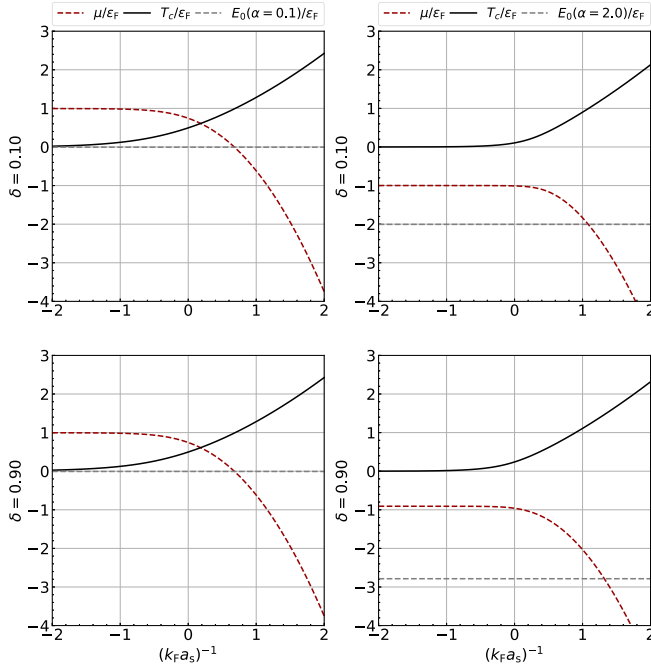


FIG. 8. Finite T mean-field parameters for intraband superconductor as functions of $(k_F a_s)^{-1}$, here for mass difference $\delta = 0.8$ and different values of the hybridization strength α .

where the excitation energies $\epsilon_{\mathbf{k}}^{\pm} = \sqrt{B_{\mathbf{k}} \pm \sqrt{B_{\mathbf{k}}^2 - C_{\mathbf{k}}}}$, with

$$B_{\mathbf{k}} \equiv \frac{(\xi_{\mathbf{k}}^f)^2 + (\xi_{\mathbf{k}}^d)^2 + \Omega_0^2}{2} + |V_{\mathbf{k}}|^2, \quad (D2)$$

$$C_{\mathbf{k}} \equiv (\xi_{\mathbf{k}}^f \xi_{\mathbf{k}}^d - |V_{\mathbf{k}}|^2)^2 + (\xi_{\mathbf{k}}^d)^2 \Omega_0^2.$$

Together with the occupation number equation

$$n(T) = \sum_{\mathbf{k}, \eta} \left[1 - \frac{1}{\epsilon_{\mathbf{k}}^{\eta}} \frac{D_{\mathbf{k}}^{\eta} + \xi_{\mathbf{k}}^d \Omega_0^2}{(\epsilon_{\mathbf{k}}^{\eta})^2 - (\epsilon_{\mathbf{k}}^{-\eta})^2} \tanh\left(\frac{\epsilon_{\mathbf{k}}^{\eta}}{2T}\right) \right], \quad (D3)$$

where $D_{\mathbf{k}}^{\eta} \equiv 2\xi_{\mathbf{k}}[(\epsilon_{\mathbf{k}}^{\eta})^2 + \xi_{\mathbf{k}}^f \xi_{\mathbf{k}}^d - |V_{\mathbf{k}}|^2]$, this provides a closed set of equations, which is next solved numerically for finite temperatures T .

Figures 8 and 9 compare the mean-field gap function and chemical potential as functions of the scattering length and hybridization, respectively. Variation of the scattering length (Fig. 8) shows results closely resembling those for the conventional single band superconductors, while variation of the hybridization (Fig. 9) has different implications. That is, differently from the interband case, the hybridization suppressed pair correlations as evident from the suppression of T_c with increasing α (see main panels of Fig. 9). Further, we notice that the chemical potential never falls below the band bottom, $\mu > E_0$, when α is used as the tuning parameter (compare Fig. 8 and insets of Fig. 9).

APPENDIX E: SCALING OF THE CRITICAL TEMPERATURE

As discussed in Sec. III B, the critical temperature appears to show some scaling as a function of α and δ . $T_c(\alpha, \delta)$

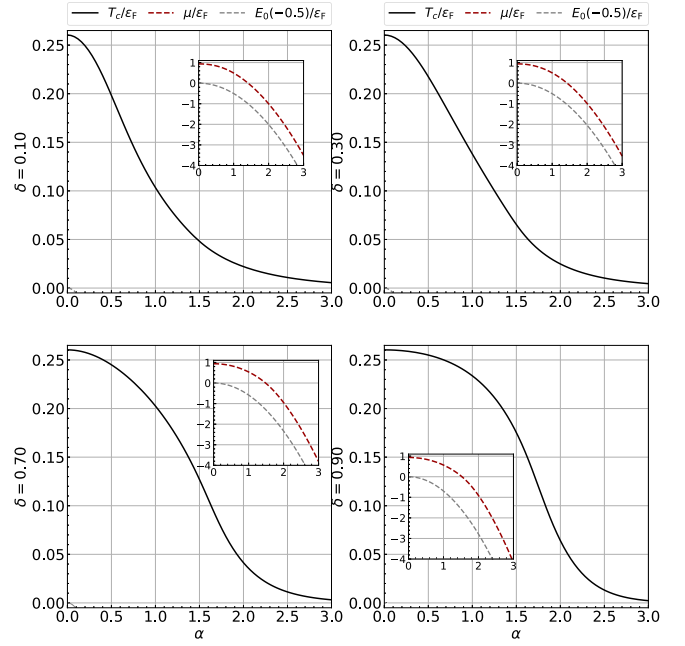


FIG. 9. Finite T mean-field parameters for intraband superconductor as functions of the hybridization strength α , for different values of mass difference δ and scattering length $(k_F a_s)^{-1} = -0.5$.

decreases, respectively, increases in the weak and strong coupling regimes (i.e., for small, respectively, large values of α) as δ increases. This can be seen in the left Fig. 10 for the scattering length $(k_F a_s)^{-1} = -0.5$. Interestingly, the curves $T_c(\alpha)$ for different δ values all intersect in $\alpha_0 \simeq 1.08$, indicating some form of scaling. In the right Fig. 10 we show the result for a simple scaling ansatz

$$\frac{T_c(\alpha, \delta)}{T_c(\alpha_0, \delta)} = F\left(\frac{\delta}{|\alpha - \alpha_0|^p}\right), \quad (E1)$$

where we find an (approximate) collapse for $p = -1/3$. This indicates irrelevance of δ in the vicinity of the crossing point α_0 , and a line of constant T_c for $\delta = C|\alpha - \alpha_0|^p$, with C some constant. At this point we do not have a deeper understanding of this (approximate) scaling.

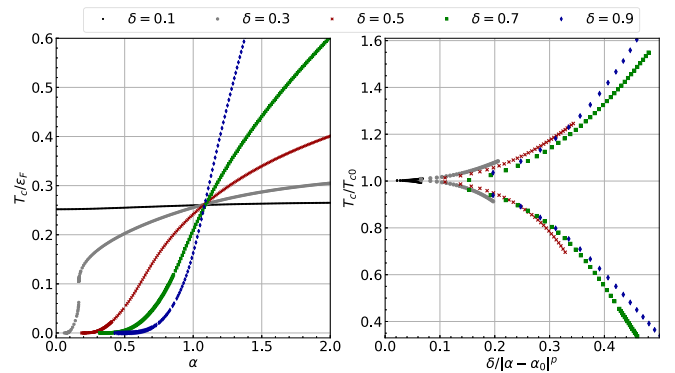


FIG. 10. Left: Mean-field critical temperature as a function of the hybridization for scattering length $(k_F a_s)^{-1} = -0.5$ and different values of δ . All T_c curves intersect in $\alpha_0 \simeq 1.08$. Right: Same data, now using the scaling ansatz Eq. (E1) with $p = -1/3$.

- [1] H. Suhl, B. T. Matthias, and L. R. Walker, *Phys. Rev. Lett.* **3**, 552 (1959).
- [2] J. Kondo, *Progr. Theor. Phys.* **29**, 1 (1963).
- [3] D. C. Johnston, *Adv. Phys.* **59**, 803 (2010).
- [4] G. R. Stewart, *Rev. Mod. Phys.* **83**, 1589 (2011).
- [5] E. Dagotto, *Rev. Mod. Phys.* **85**, 849 (2013).
- [6] P. C. Dai, J. P. Hu, and E. Dagotto, *Nat. Phys.* **8**, 709 (2012).
- [7] J. Paglinone and R. L. Greene, *Nat. Phys.* **6**, 645 (2010).
- [8] P. J. Hirschfeld, M. M. Korshunov, and I. I. Mazin, *Rep. Prog. Phys.* **74**, 124508 (2011).
- [9] A. V. Chubukov, *Annu. Rev. Condens. Matter Phys.* **3**, 57 (2012).
- [10] S. Tsuda, T. Yokoya, T. Kiss, Y. Takano, K. Togano, H. Kito, H. Ihara, and S. Shin, *Phys. Rev. Lett.* **87**, 177006 (2001).
- [11] X. K. Chen, M. J. Konstantinović, J. C. Irwin, D. D. Lawrie, and J. P. Franck, *Phys. Rev. Lett.* **87**, 157002 (2001).
- [12] F. Giubileo, D. Roditchev, W. Sacks, R. Lamy, D. X. Thanh, J. Klein, S. Miraglia, D. Fruchart, J. Marcus, and P. Monod, *Phys. Rev. Lett.* **87**, 177008 (2001).
- [13] P. Szabó, P. Samuely, J. Kacmarčík, T. Klein, J. Marcus, D. Fruchart, S. Miraglia, C. Marcenat, and A. G. M. Jansen, *Phys. Rev. Lett.* **87**, 137005 (2001).
- [14] H. D. Yang, J.-Y. Lin, H. H. Li, F. H. Hsu, C. J. Liu, S.-C. Li, R.-C. Yu, and C.-Q. Jin, *Phys. Rev. Lett.* **87**, 167003 (2001).
- [15] F. Bouquet, R. A. Fisher, N. E. Phillips, D. G. Hinks, and J. D. Jorgensen, *Phys. Rev. Lett.* **87**, 047001 (2001).
- [16] Y. Wang, T. Plackowski, and A. Junod, *Physica C* **355**, 179 (2001).
- [17] A. M. Black-Schaffer and A. V. Balatsky, *Phys. Rev. B* **88**, 104514 (2013).
- [18] S. Raghu, X.-L. Qi, C.-X. Liu, D. J. Scalapino, and S.-C. Zhang, *Phys. Rev. B* **77**, 220503(R) (2008).
- [19] A. Moreo, M. Daghofer, J. A. Riera, and E. Dagotto, *Phys. Rev. B* **79**, 134502 (2009).
- [20] A. Moreo, M. Daghofer, A. Nicholson, and E. Dagotto, *Phys. Rev. B* **80**, 104507 (2009).
- [21] A. Moreo and E. Dagotto, *Phys. Rev. B* **100**, 214502 (2019).
- [22] O. V. Dolgov, E. P. Fetsiov, D. I. Khomskii, and K. Svozil, *Z. Phys. B* **67**, 63 (1987).
- [23] O. V. Dolgov, E. P. Fetsiov, and D. I. Khomskii, *Phys. Lett. A* **125**, 267 (1987).
- [24] J. Tahir-Kheli, *Phys. Rev. B* **58**, 12307 (1998).
- [25] W. V. Liu and F. Wilczek, *Phys. Rev. Lett.* **90**, 047002 (2003).
- [26] E. Gubankova, W. V. Liu, and F. Wilczek, *Phys. Rev. Lett.* **91**, 032001 (2003).
- [27] F. Deus, M. A. Continentino, and H. Caldas, *Ann. Phys.* **362**, 208 (2015).
- [28] J. Bardeen, L. N. Cooper, and J. R. Schrieffer, *Phys. Rev.* **108**, 1175 (1957).
- [29] F. Dalfovo, S. Giorgini, L. P. Pitaevskii, and S. Stringari, *Rev. Mod. Phys.* **71**, 463 (1999).
- [30] S. Rinott, K. B. Chashka, A. Ribak, E. D. L. Rienks, A. Taleb-Ibrahimi, P. Le Fevre, F. Bertran, M. Randeria, and A. Kanigel, *Sci. Adv.* **3**, e1602372 (2017).
- [31] H. Tajima, A. Perali, and P. Pieri, *Condens. Matter* **5**, 10 (2020).
- [32] M. Iskin and C. A. R. Sá de Melo, *Phys. Rev. A* **76**, 013601 (2007).
- [33] G. Orso, L. P. Pitaevskii, and S. Stringari, *Phys. Rev. A* **77**, 033611 (2008).
- [34] R. B. Diener and M. Randeria, *Phys. Rev. A* **81**, 033608 (2010).
- [35] R. Hanai, T. Kashimura, R. Watanabe, D. Inotani, and Y. Ohashi, *Phys. Rev. A* **88**, 053621 (2013).
- [36] See, e.g., Ref. [37], showing that for a multiband, *s*-wave superconductor, with occupation close to two electrons per atom, even parity hybridization leads to a superconducting quantum critical point. We thus expect that in this case superconductivity is destroyed before the crossover to a strong coupling regime can be realized.
- [37] D. Reyes, N. Lopes, M. A. Continentino, and Ch. Thomas, *Phys. Rev. B* **99**, 224514 (2019).
- [38] S. M. Ramos, M. B. Fontes, E. N. Hering, M. A. Continentino, E. Baggio-Saitovich, F. D. Neto, E. M. Bittar, P. G. Pagliuso, E. D. Bauer, J. L. Sarrao, and J. D. Thompson, *Phys. Rev. Lett.* **105**, 126401 (2010).
- [39] C. Wang, Y. Y. Zhang, and Q. H. Chen, *Phys. Rev. A* **85**, 052112 (2012).
- [40] L. He, X. G. Huang, H. Hu, and X. J. Liu, *Phys. Rev. A* **87**, 053616 (2013).
- [41] J. Lee and D. H. Kim, *Phys. Rev. A* **95**, 033609 (2017).
- [42] Z. Q. Yu and H. Zhai, *Phys. Rev. Lett.* **107**, 195305 (2011).
- [43] Jayantha P. Vyasankere and Vijay B. Shenoy, *Phys. Rev. A* **86**, 053617 (2012).
- [44] H. Shi, P. Rosenberg, S. Chiesa, and S. Zhang, *Phys. Rev. Lett.* **117**, 040401 (2016).
- [45] M. Gong, S. Tewari, and C. Zhang, *Phys. Rev. Lett.* **107**, 195303 (2011).
- [46] A. J. Leggett, *Modern Trends in the Theory of Condensed Matter*, edited by A. Pekalski and J. Przystawa (Springer Verlag, Berlin, 1980).
- [47] A. J. Leggett, *J. Phys. Collo.* **41**, C7-19 (1980).
- [48] P. Nozières and S. Schmitt-Rink, *J. Low Temp. Phys.* **59**, 3 (1985).
- [49] C. A. R. Sa de Melo, M. Randeria, and J. R. Engelbrecht, *Phys. Rev. Lett.* **71**, 3202 (1993).
- [50] J. R. Engelbrecht, M. Randeria, and C. A. R. Sá de Melo, *Phys. Rev. B* **55**, 15153 (1997).
- [51] R. B. Diener, R. Sensarma, and M. Randeria, *Phys. Rev. A* **77**, 023626 (2008).
- [52] N. N. Bogoliubov, *Sov. Phys. JETP* **11**, 23 (1947).
- [53] For the calculation it is convenient to choose the *z* axis along the vector $(1, 1, \gamma)$, defining the hybridization, such that $V_{\mathbf{k}}^2 = \alpha^2(2 + \gamma^2)k_z^2$.
- [54] A. Altland and B. Simons, *Condensed Matter Field Theory* (Cambridge University Press, Cambridge, 2010).
- [55] J. Negele and H. Orland, *Quantum Many-Particle Systems* (Addison-Wesley Pub. Co., Redwood City, 1988).